Literature Seminar '05 6/22 Wed.

Ryo Takita (P3)

☆ Assembled Molecules and New Functions : Implications for a Sophisticated Asymmetric Catalysis

with high total efficiency
- high reactivity
- high selectivity (ee, substrates)
- easy operation and preparation
- low catalyst loading
- ⋮
- etc.

· Assembled Catalyst

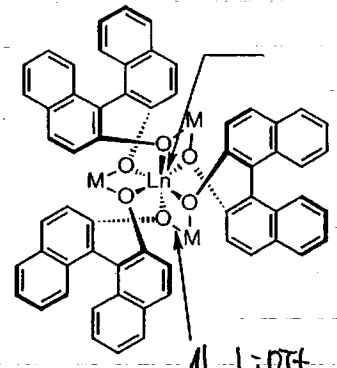

⇂ LiOTf
Vijay's cat.

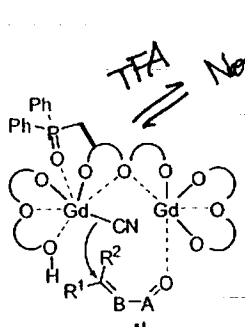

⇂
4:5 complex?

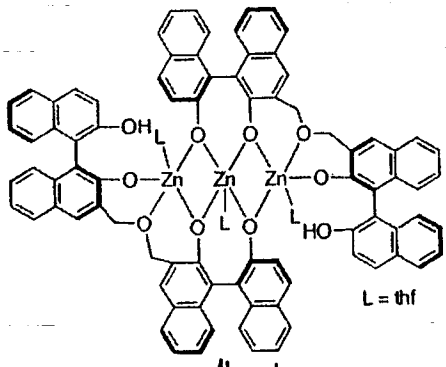

⇂ ketone
3:7:4 complex.

· self-assemble → catalyst components
- structural change → · new function · higher performance

→ catalyst + substrates
- proximity effects
- activation

☆ Another Aspect : Artificial Biomolecule → Biochemistry

< Contents >
(1) Combined with Allosteric Effects
(2) Catalysis in Supramolecule : Defined Cavity
(3) Dual Activation on One Substrate
(4) Chirality Transfer
(5) Chiral Metallacyclophane
(6) Artificial Ion Channel.

(Actually, all of them have been achieved by our group.)

allo + steric

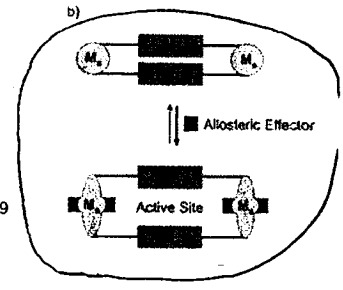

• (1) Combined with Allosteric Effects

A Supramolecular Approach to an Allosteric Catalyst

J. AM. CHEM. SOC. 2003, 125, 10508−10509

Nathan C. Gianneschi,† Paul A. Bertin,† SonBinh T. Nguyen,† Chad A. Mirkin,*,† Lev N. Zakharov,‡ and Arnold L. Rheingold‡

Scheme 1. The Supramolecular Allosteric Catalyst[a]

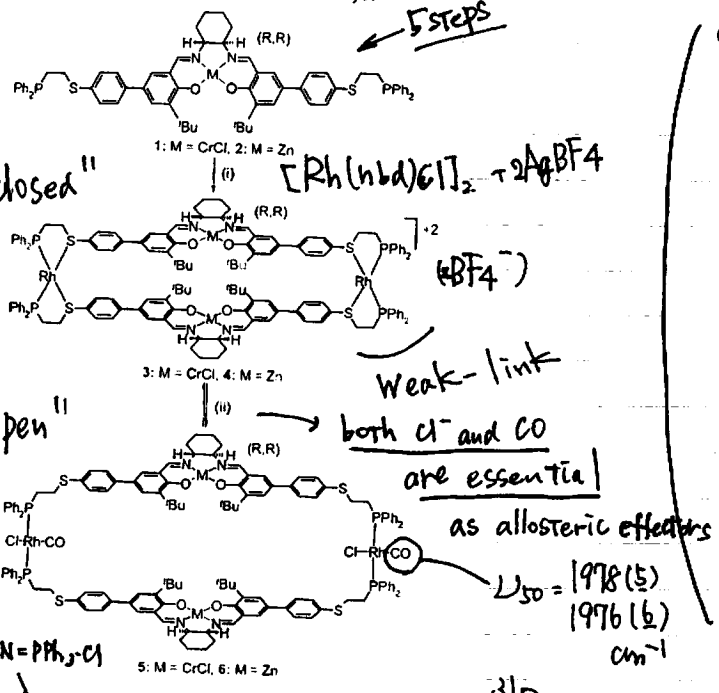

[a] Counterions are BF_4^-. Reagents and solvents: (i) $Rh(norbornadiene)_2BF_4$, CH_2Cl_2; (ii) PPNCl/CO, benzonitrile; 3 and 4 may be synthesized from 5 and 6, respectively, by the removal of CO in vacuo or by N_2 purge.

cf. Acc. Chem. Res. 2000, 33, 421.
E.N. Jacobsen et al.

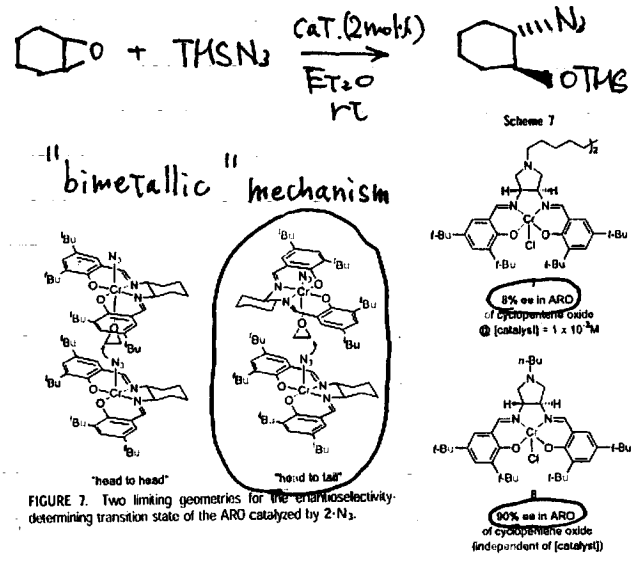

FIGURE 7. Two limiting geometries for the enantioselectivity-determining transition state of the ARO catalyzed by 2·N_3.

^{31}P NMR → Trans-phosphine complex.
(a single peak)

in benzonitrile →
(3: 68% ee
7: 12% ee

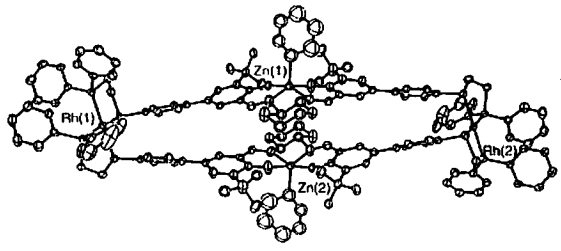

Figure 1. Thermal ellipsoid drawing of 4-(pyridine)$_2$·CH_2Cl_2 showing the labeling scheme for selected atoms and elipsoids at 30% probability. Hydrogen atoms are omitted for clarity. Zn−Zn distance: 5.24 Å. Rh−Rh distance: 24.66 Å.

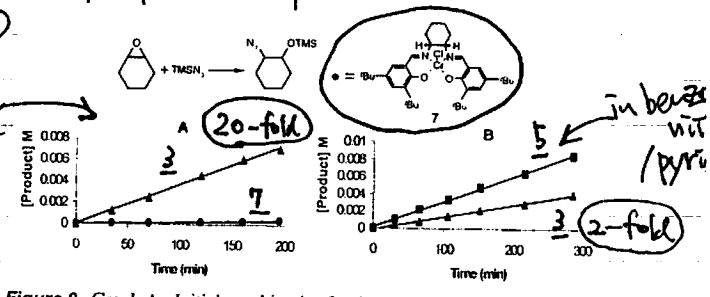

Figure 2. Graph A: Initial rate kinetics for the ring opening of cyclohexene oxide by $TMSN_3$ catalyzed by 3 (▲) (2.6 mM) and a monomeric Cr(III)-salen complex 7 (●) (5.2 mM) in benzonitrile at room temperature. The catalyst concentrations are the same with respect to Cr(III). Graph B: Initial rate kinetics for the ring opening of cyclohexene oxide by $TMSN_3$, as catalyzed by 3 (▲) and 5 (■) each at 2.6 mM, in benzonitrile/pyridine at room temperature.

cf.

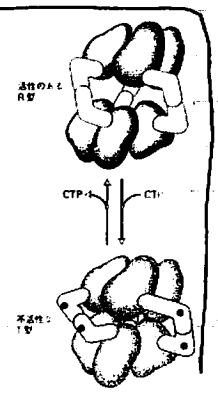

• Even the use of "closed" complex 3 showed the apperant acceleration in cooperative catalysis.

• "Open" complex should provide more suitable environment via allostellic regulation.

Reversibly Addressing an Allosteric Catalyst In Situ: Catalytic Molecular Tweezers**

*Nathan C. Gianneschi, So-Hye Cho, SonBinh T. Nguyen, and Chad A. Mirkin**

Angew. Chem. Int. Ed. 2004, 43, 5503–5507

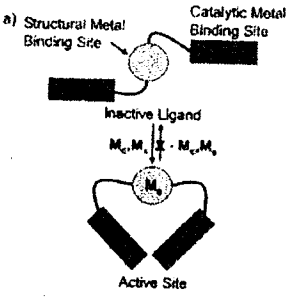

3

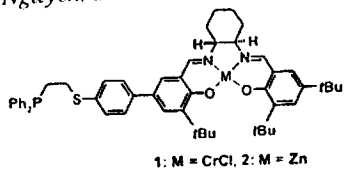

1: M = CrCl, 2: M = Zn

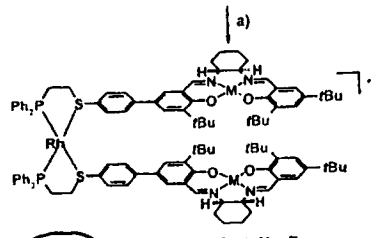

3: M = CrCl, 4: M = Zn

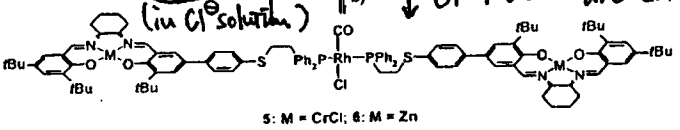

5: M = CrCl; 6: M = Zn

Scheme 2. Synthesis of the allosteric tweezer complexes. Counterions are BF_4^-. All cyclohexyl salen backbones have (*R,R*) stereochemistry. Reagents and solvents; a) $[Rh(NBD)_2]BF_4$, CH_2Cl_2; b) PPNCl/CO (PPNCl = bis(triphenylphosphoranylidene)ammonium chloride); 3 and 4 may be synthesized from 5 and 6, respectively, by the removal of CO in vacuo or by purging with N_2.

Table 1: Selectivity data for the ring opening of cyclohexene oxide by $TMSN_3$ catalyzed by 3, 5, and the monomeric Cr^{III}–salen complex 7.[a]

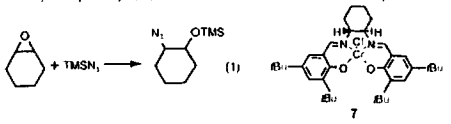

7

Entry	Catalyst	[Catalyst] M 1×10^{-3}	% *ee* of product[b]
1	3	7.2	80
2	5	7.2	74
3	7	7.2	26
4	3	4.7	80
5	5	4.7	73
6	3	3.6	79
7	5	3.6	68
8	7	3.6	12
9	3	2.5	77
10	5	2.5	60
11	3	1.8	72
12	5	1.8	54
13	3	0.72	65
14	5	0.72	44
15	3	0.36	63
16	5	0.36	32
17	3	0.14	49
18	5	0.14	21

[a] All reactions were performed at room temperature in THF. [b] %*ee* of 1-azido-2-(trimethylsiloxy)cyclohexane was determined by chiral GC.

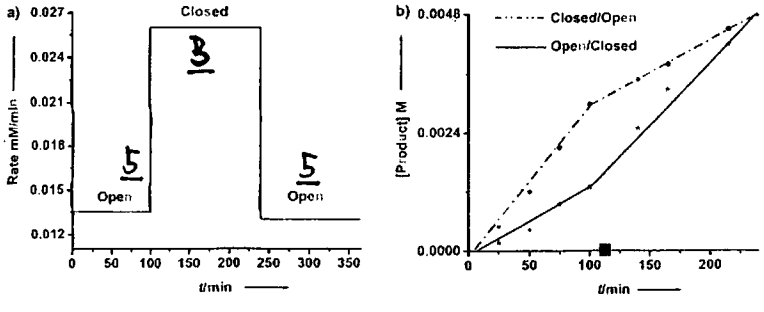

Figure 2. In situ reversibility of the catalysis. a) The catalyst being taken through an open/closed/open cycle. b) The switch point (■) indicates CO saturation or CO desaturation (N_2 purge) points at which the catalyst is opened (complex 5 from complex 3) or closed (complex 3 from complex 5) respectively. Reaction conditions: Cyclohexene oxide (6.1 mmol), $TMSN_3$ (2.3 mmol), 3.6 mM catalyst in benzonitrile at room temperature (see Supporting Information for details).

in Nature, Allosteric regulation is reversible.

(cf.) Jacobsen et al. JACS, 1998, 120, 10780.

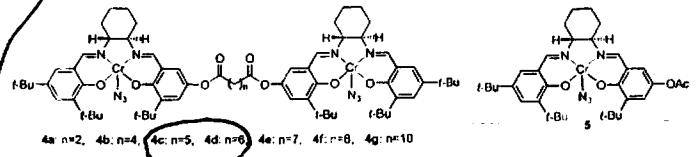

4a: n=2, 4b: n=4, 4c: n=5, 4d: n=6, 4e: n=7, 4f: n=8, 4g: n=10

→ highest reactivity via intramolecular mechanism.

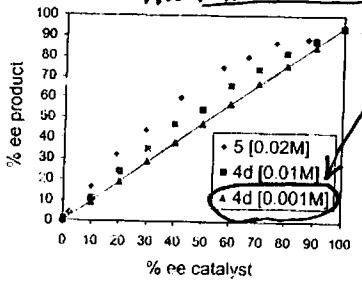

at low concentration, there was a strict linear relationship.

Figure 4. Nonlinear effects in the ARO of cyclopentene oxide with $TMSN_3$ catalyzed by 5 and 4d.

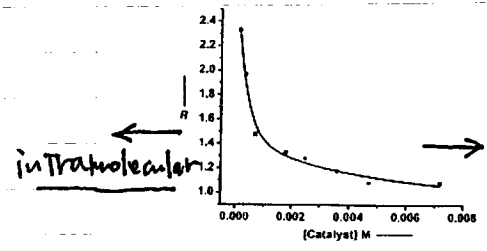

intramolecular → intermolecular

for 5, the cooperativity of two catalytic centers is reduced, thus rendering the catalyst less selective.

Figure 3. The allosteric effect expressed in terms of selectivity. *R* is the allosteric selectivity ratio = (%*ee* of the product formed by using 3):(%*ee* of the product formed by using 5).

cf. Angew. Chem., Int. Ed. 2002, 41, 3626.

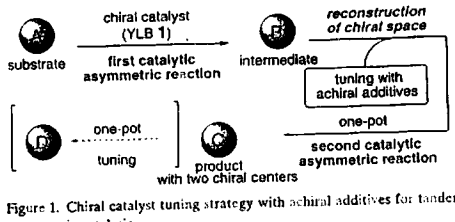

Figure 1. Chiral catalyst tuning strategy with achiral additives for tandem asymmetric catalysis.

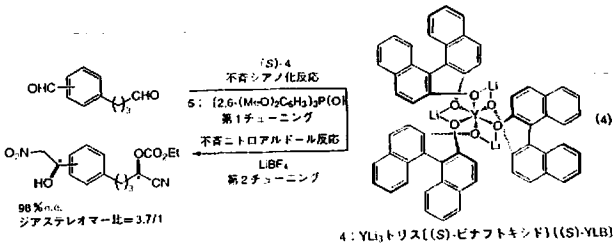

Signal Amplification and Detection via a Supramolecular Allosteric Catalyst

Nathan C. Gianneschi, SonBinh T. Nguyen, and Chad A. Mirkin*

J. AM. CHEM. SOC. 2005, 127, 1644–1645

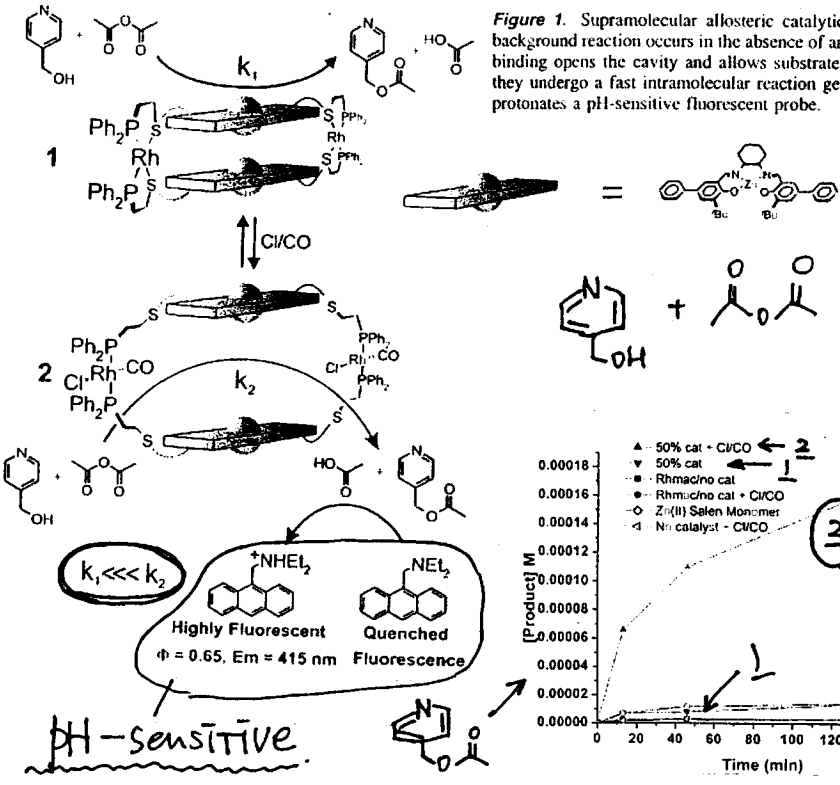

Figure 1. Supramolecular allosteric catalytic signal amplifier. A slow background reaction occurs in the absence of analyte (Cl^- or CO). Analyte binding opens the cavity and allows substrate molecules to enter, where they undergo a fast intramolecular reaction generating acetic acid, which protonates a pH-sensitive fluorescent probe.

Allosteric Control in Catalytic Detection

bimetallic

proximity effects

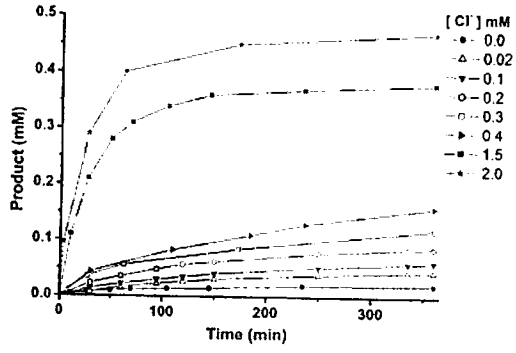

Figure 2. Product (4-acetoxymethylpyridine) concentration vs time for a range of Cl^- ion concentrations. Reactions were monitored by GC. Conditions: CH_2Cl_2, rt, 1 mM pyridyl carbinol, 1 mM acetic anhydride, 1.5 mM biphenyl (standard), 1 mM closed catalyst, CO (1 atm), and appropriate amounts of benzyltriethylammonium chloride.

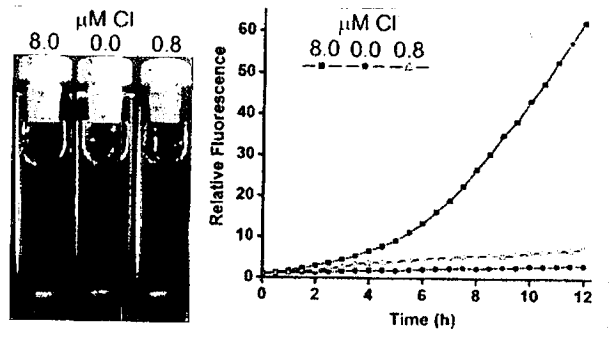

Figure 3. Photo: Taken under a UV lamp (365 nm); reaction time = 6 h. Graph: Fluorescence vs time plot (λ_{ex} = 368 nm, λ_{em} = 415 nm). Conditions: 0.1 mM catalyst, 0.1 mM pyridyl carbinol, 0.1 mM acetic anhydride, 1 mM diethylaminomethylanthracene, CH_2Cl_2, rt, benzyltriethylammonium chloride.

Shinkai et al. Chem. Commun. 2004, 420. "artificial phosphodiesterase"

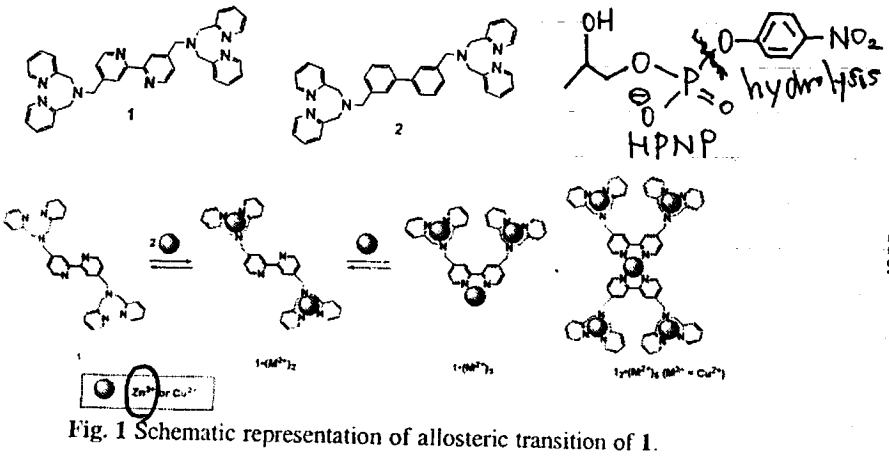

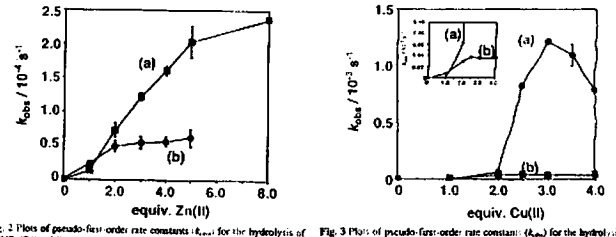

Fig. 2 Plots of pseudo-first-order rate constants (k_{obs}) for the hydrolysis of HPNP (0.8 mM) at various Zn^{2+} concentrations in 33% ethanol/water (HEPES, 25 mM): (a) [1] = 0.1 mM, (b) [2] = 0.1 mM, pH 7.7 at 25 °C.

Fig. 3 Plots of pseudo-first-order rate constants (k_{obs}) for the hydrolysis of HPNP (1.0 mM) at various Cu^{2+} concentrations in 33% ethanol/water (HEPES, 25 mM): (a) [1] = 1.0 mM, (b) [2] = 1.0 mM, pH 7.7 at 25 °C. Inset is an enlarged view for 2 and Cu^{2+}.

1 with 3equiv. of Cu^{2+}

$[1\cdot(Cu^{2+})_3]/[1_2\cdot(Cu^{2+})_5]/[1\cdot(Cu^{2+})_2]$

= 81 / 11 / 8

Fig. 1 Schematic representation of allosteric transition of 1.

The Bis-Barium Complex of a Butterfly Crown Ether as a Phototunable Supramolecular Catalyst

J. AM. CHEM. SOC. 2003, 125, 2224-2227

Roberta Cacciapaglia,* Stefano Di Stefano, and Luigi Mandolini*

ct.)

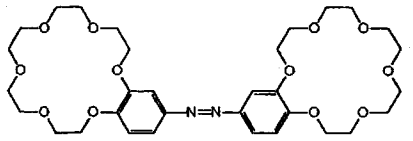

1

azobis(benzo-18-c-6) ether

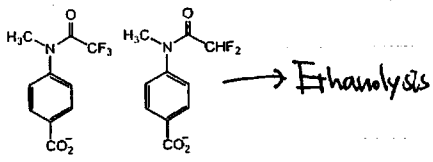

2 3

→ Ethanolysis

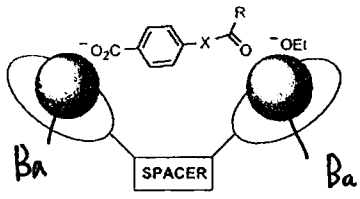

X = N(Me), O

Figure 1. Productive catalyst–substrate complex for the basic ethanolysis of esters and anilides. One of the metal ions serves as a binding unit for the carboxylate anchoring group, and the other delivers an activated ethoxide ion to the substrate carbonyl.

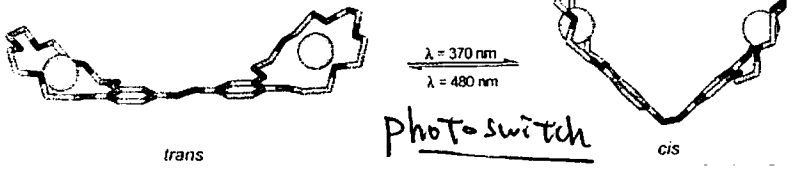

photo-switch

Figure 4. Computer-generated structures of interswitchable trans and cis forms of 1·[Ba]$_2$.

Molecules That Assemble by Sound: An Application to the Instant Gelation of Stable Organic Fluids

Takeshi Naota* and Hiroshi Koori

JACS, ASAP (Web release June 11, 2005)

ct.

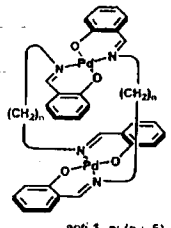

anti-1 a: (n = 5)
b: (n = 6)
c: (n = 7)
d: (n = 8)

Figure 1. anti-1a in acetone at 293 K. (a) A long-lived, stable solution under nonsonication conditions. (b) A gel just after presonication (0.45 W/cm^2, 40 kHz, 3 s).

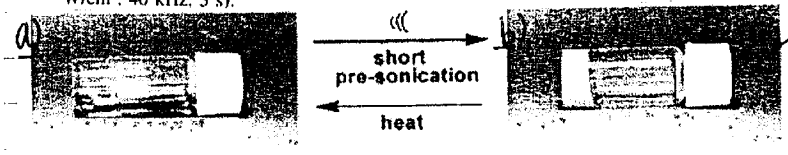

please see the movie (mpeg) in Supporting Information.

1b-1d
↳ no gel formation.

bent, self-lock

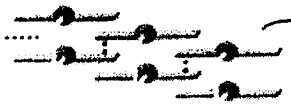

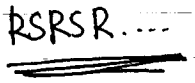

planar, interlock

• pure (−)-anti-1a (100% ee) → no gel formation.

↓

42% ee, 1.5×10^{-2} M in benzene.

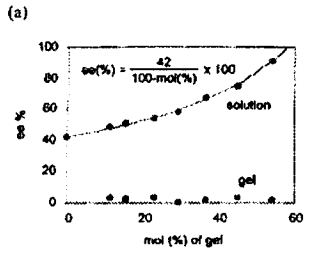

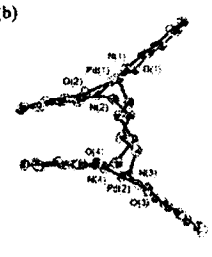

Figure 3. (a) Enantiomer excess of *anti*-1a in the partial gel (red dots) and the remaining solution (blue dots), obtained during the gelation of a 1.50×10^{-2} M solution of (−)-*anti*-1a (42% ee) in benzene after presonication (0.45 W/cm^2, 40 kHz, 10 s). (b) Molecular structure of *anti*-1a showing intramolecular π-stacking of the cofacial bent coordination blades. Side view of (R)-form. Selected bond distances (Å) and angles (deg): Pd(1)−O(1), 2.002(7); Pd(1)−O(2), 1.986(6); Pd(1)−N(1), 2.015(8); Pd(1)−N(2), 2.023(8); O(1)−Pd(1)−N(1), 91.3(3); O(2)−Pd(1)−N(2), 90.4(3); C(2)−N(2)−Pd(1)−O(2), 22.6(8); C(4)−N(4)−Pd(2)−O(4), 15.7(8).

(2). Catalysis in Supramolecule - Defined Cavity

Host–Guest Systems VIP

- **Supramolecular Catalysis of a Unimolecular Transformation: Aza-Cope Rearrangement within a Self-Assembled Host****

Dorothea Fiedler, Robert G. Bergman, and Kenneth N. Raymond**

Angew. Chem., Int. Ed. 2004, 43, 6748.
Acc. Chem. Res. 2005, 38, 351.

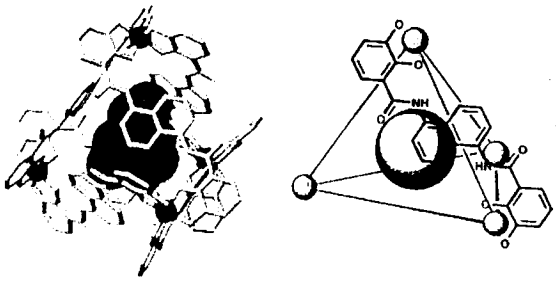

FIGURE 1. Model (left) of the crystal structure of $[NEt_4 \subset Fe_4L_6]^{11-}$ and schematic (right) of $[G \subset M_4L_6]^{11-}$. Six bis-bidentate catechol amide ligands span the edges of the tetrahedron (only one of the ligands is drawn for clarity).

- Difficulty in Supramolecular Catalysis: a problem that frequently occurs when the cavity binds the reaction product more strongly than the substrate

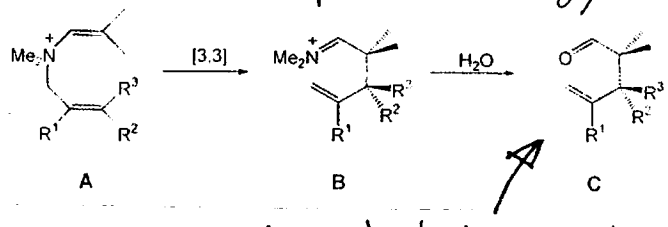

neutral molecules are only very weakly bound by the supramolecular host.
→ leading to catalyst Turnover?

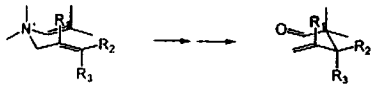

substrate	R_1	R_2	R_3	k_{free} [x 10^{-5} s^{-1}]	$k_{encaps.}$ [x 10^{-5} s^{-1}]	acceleration
13a	H	H	H	3.49	16.3	5
13b	Me	H	H	7.61	198	26
13c	H	Et	H	3.17	446	141
13d	H	H	Et	1.50	135	90
13e	H	*n*-Pr	H	4.04	604	150
13f	H	H	*n*-Pr	1.69	74.2	44
13g	H	*i*-Pr	H	0.37	316	854

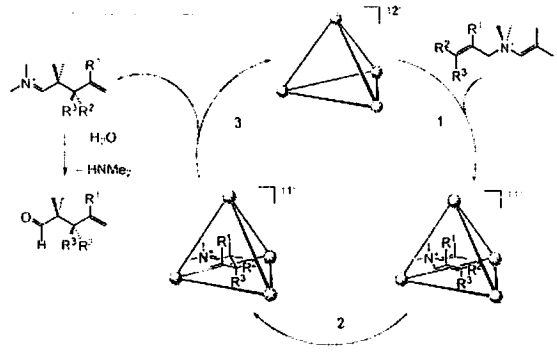

Figure 4. Proposed catalytic cycle for the cationic 3-aza-Cope rearrangement.

13c: free rearr. $\Delta H^{\ddagger} = 23.1 \pm 0.8$ kcal/mol
$\Delta S^{\ddagger} = -8 \pm 2$ e.u. (1 e.u. = 4.184 $JK^{-1}mol^{-1}$)
→ chairlike Transition (highly organized)

encapsulated rearr. $\Delta H^{\ddagger} = 23.0 \pm 0.9$ kcal/mol
$\Delta S^{\ddagger} = 2 \pm 3$ e.u. → • Upon encapsulation, the substrate loses several rotational degrees of freedom and appears to be preorganized into a reactive conformation.

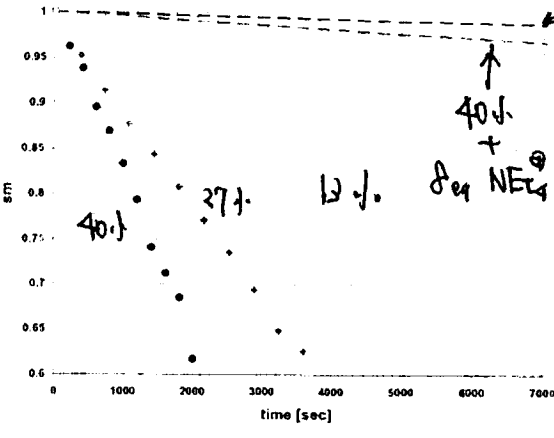

FIGURE 6. Initial rates (plotted as disappearance of starting material (SM) in mole fraction) at 25 °C for the catalytic 3-Aza Cope rearrangement of **13c**: (●) 40% catalyst loading; (◆) 27% catalyst loading; (▲) 13% catalyst loading; (red, – – –) 40% catalyst loading inhibited with 8 equiv NEt_4^+; (black, – – –) uncatalyzed reaction.

⇨ enantioselective variants using homochiral assemblies ($\Delta\Delta\Delta\Delta$ or $\Lambda\Lambda\Lambda\Lambda$)

Wacker Oxidation in an Aqueous Phase through the Reverse Phase-Transfer Catalysis of a Self-Assembled Nanocage

Hirokazu Ito, Takahiro Kusukawa,*[†] and Makoto Fujita*[†,‡]

Chem. Lett. 2000. 598.

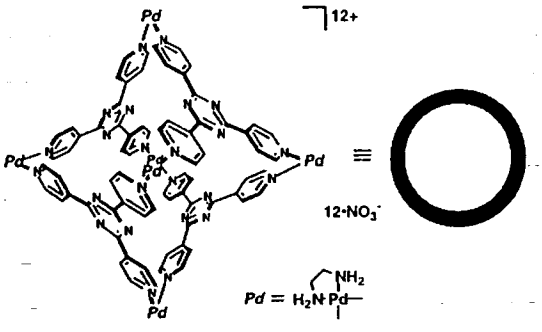

1

Table 1. Aerobic oxidation of styrene and its derivatives catalyzed by **1** and **2**

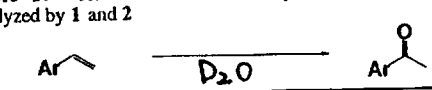

Run	Ar	1 / mol%	2 / mol%	Yield of ketones /%[b]
1	phenyl	10	10	82
2	phenyl	-	10	4
3[a]	phenyl	10	10	3
4	phenyl	10	-	4
5	*p*-methoxyphenyl	10	10	53
6	*p*-tolyl	10	10	64
7	*p*-nitrophenyl	10	10	13
8	2-naphthyl	10	10	12

[a] 1,3,5-Trimethoxybenzene (1 equiv to styrene) was added. [b] Determined by ^{1}H NMR.

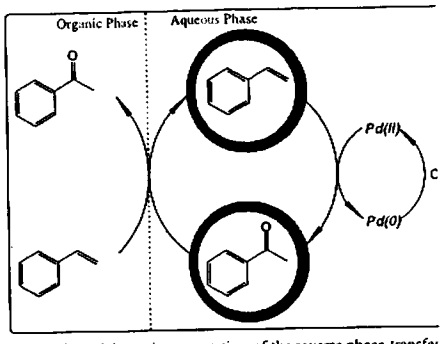

Figure 2. Schematic presentation of the reverse phase-transfer catalysis of **1** for the Wacker oxidation of styrene.

2 : (en) $Pd(NO_3)_2$

Cu^{II} is not required.

Artificial Enzymes Formed through Directed Assembly of Molecular Square Encapsulated Epoxidation Catalysts**

Melissa L. Merlau, Maria del Pilar Mejia, SonBinh T. Nguyen,* and Joseph T. Hupp*

Angew. Chem., Int. Ed. 2001, 40, 4239

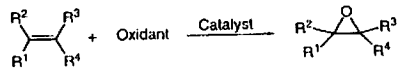

(1)

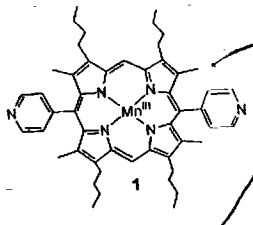

1

there is a complete loss of activity after about 50 catalytic cycles.
→ the formation of an oxo-bridged dimer (Mn-O-Mn)

(cf.) cytochrome P450
- potent catalytic center
- a surrounding protein superstructure

encapsulation of cat 1 in a supramolecular cavity

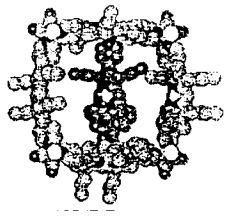

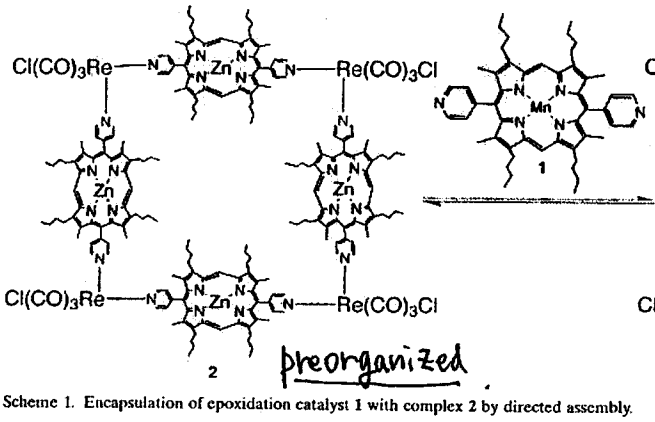

2 preorganized

1

1+2

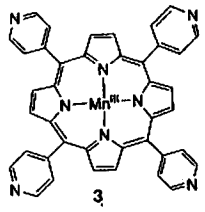

3

more strongly complexed catalyst

Scheme 1. Encapsulation of epoxidation catalyst **1** with complex **2** by directed assembly.

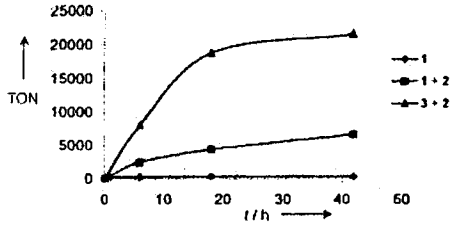

Figure 2. The enhanced stability and enhanced TONs of the catalyst assemblies [1+2] and [3+2] compared to the free catalyst **1**.

preferential binding of aromatic substrates

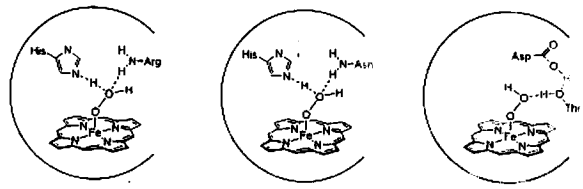

Figure 1. Comparison of proposed proton-activated O–O bond cleavage for iron-oxo heme formation in (a) peroxidases, (b) catalases, and (c) cytochrome P450 monooxygenases.

(3) · Dual Activation on One Substrate

ex.) **Hangman Salophens** J. AM. CHEM. SOC. 2005, *127*, 5278–5279

Shih-Yuan Liu and Daniel G. Nocera*

see also : JACS, 2003, 125, 1866.
JACS, 2001, 123, 1513.

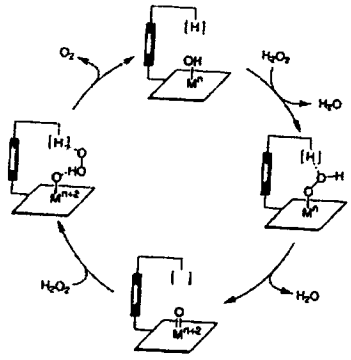

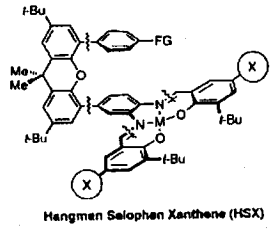

HSX-^{t}Bu : FG = CO_2H
EHSX-^{t}Bu : FG = CO_2Me

Table 1. Turnover Numbers for the Dismutation of H_2O_2 Catalyzed by Manganese Salophen Complexes

catalyst	O_2 yield/TON[a]
Mn–HSX-*t*Bu	4372
Mn–EHSX-*t*Bu	98
Mn–EHSX-*t*Bu[b]	373
Mn–Saloph-*t*Bu	86
Mn–Saloph-*t*Bu[b]	472
$Mn(OAc)_2 \cdot 2H_2O$	62

[a] After 1 h. [b] In presence of 1 equiv of benzoic acid.

PCET : proton-coupled electron transfer catalysis

cf. J. AM. CHEM. SOC. 2005, *127*, 4184–4185

Rapid Fixation of Methylene Chloride by a Macrocyclic Amine

Jung-Jae Lee,† Keith J. Stanger,† Bruce C. Noll,† Carlos Gonzalez,‡ Manuel Marquez,¶ and Bradley D. Smith*,†

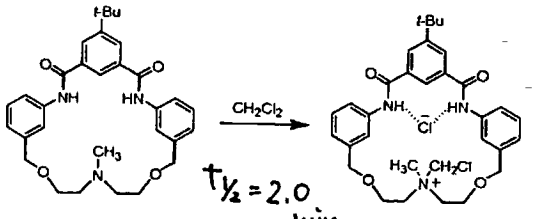

1 2 3 4

$t_{1/2}$ = 2.0 min. (298K)

$t_{1/2}$ 80000 min.

180000 min.

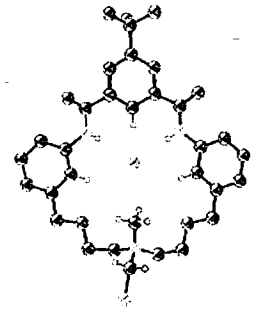

Figure 1. X-ray structure of quaternary ammonium chloride 2.

⇨ · Triple Activation?
· Dual (Dual Activation)?

(4) · Chirality Transfer

Feringa et al. Angew. Chem., Int. Ed. 2005, 44, 3230.

· Chirality transfer from large molecule to small molecule is limited.

Asymmetric Catalysis

DNA-Based Asymmetric Catalysis**

Gerard Roelfes and Ben L. Feringa**

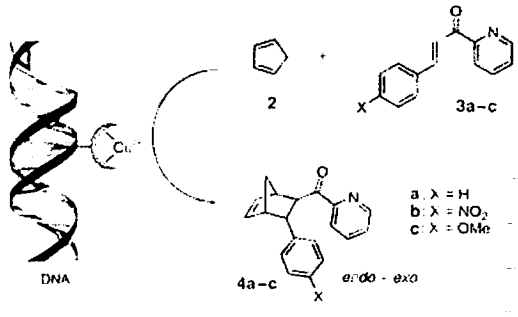

Figure 1. Schematic representation of the asymmetric Diels–Alder reaction of cyclopentadiene (2) with aza-chalcone 3, catalyzed by copper complexes of ligand 1 in the presence of DNA.

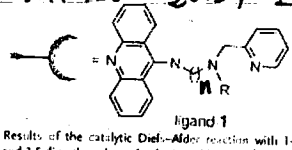

ligand 1

Table 1: Results of the catalytic Diels–Alder reaction with 1-naphthylmethyl- and 3,5-dimethoxy benzyl-substituted ligand 1[a]

Entry	Ligand 1	R	n	Dienophile	Diels–Alder Product 4 endo/exo	endo [% ee]	exo [% ee]
1	1a	n=3	3	3a	98:2	49	18
2[b]	1a		3	3a	97:3	49	23
3[c]	1a		3	3a	98:2	47	23
4	1a		3	3b	96:4	37	16
5	1a		3	3c	98:2	48	24
6	1b		4	3a	98:2	33	19
7	1c	n=5	5	3a	97:3	<5	<5
8	1d	n=2	2	3a	96:4	−48	−37
9	1e	n=3	3	3a	98:2	−37	−7
10	1f	n=2	2	3a	92:8	−37	−78
11[b]	1f		2	3a	92:8	−34	−74
12[c]	1f		2	3a	92:8	−35	−82
13[d]	1f		2	3a	82:18	−34	−80
14	1f		2	3b	88:12	−47	−78
15	1f		2	3c	91:9	−53	−90

[a] All experiments were carried out with salmon testes DNA under the standard conditions (see Experimental Section) unless noted otherwise. [b] Conditions: catalyst (0.18 mM), dienophile (4 mM), cyclopentadiene (34 mM). [c] Calf thymus DNA. [d] DNA = synthetic duplex d(GACT)$_3$-(AGTC)$_3$ (0.39 mM), cyclopentadiene (21 mM), buffer contained NaCl (75 mM).

· Instead of DNA, the use of other (smaller) molecule, such as peptide, oligo-sugars, or other usual optically active molecules is attractive for the practical use.

· Artificial Helix can be used? ex:) Prof. Yashima's research.

one of "DNAzymes"

(5) · Chiral Metallacyclophanes for Asymmetric Catalysis

Wenbin Lin et al. | JACS, 2002, 124, 12948.
Chem. Commun. 2003, 96.
OL, 2004, 6, 861.

Scheme 1

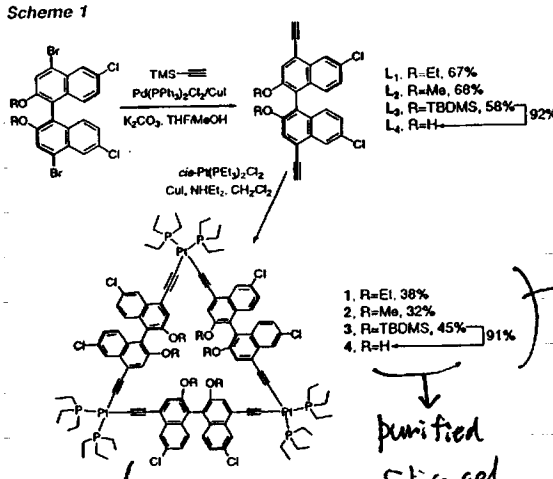

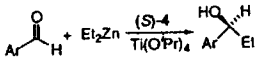

Using L4, instead of 4, the product was obtained in 80% ee.

The formation of 1–4 were confirmed by ^1H, ^{13}C, ^{31}P NMR, IR, MS, elemental analysis, UV-vis, and CD spectroscopies.

purified silica gel column chromatography

LLB ?

Table 1. Diethylzinc Additions to Aldehydes Catalyzed by Ti(IV) Complexes of 4[a]

Entry	Aldehyde	Temp	Conversion[b]	e.e. (%)[c]
1		rt	>95%	91
2		rt	>95%	91
		0 °C	>95%	92
3		rt	>95%	90
4		rt	>95%	91
5		rt	>95%	89
6		rt	>95%	90

[a] All reactions were carried out with 7 equiv of $Ti(O^iPr)_4$ (on the basis of L_4). [b] Conversion was determined by ^1H NMR. [c] ee's were determined using a Chiracel-OD HPLC column except for *p*-tolualdehyde (OJ column).

Scheme 1

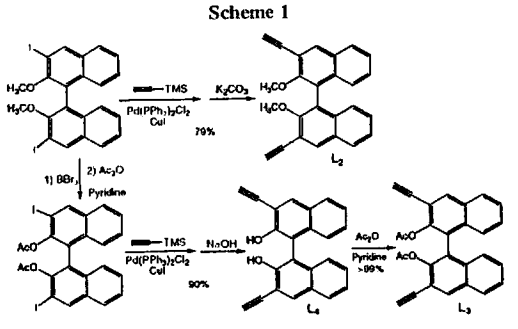

Scheme 2

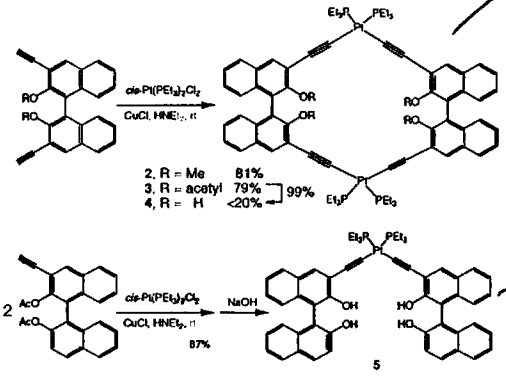

4 did not react with $Ti(O\text{-}i\text{-}Pr)_4$ to form the Ti-binolate moieties at room temperature. (see Figure 1)

more flexible

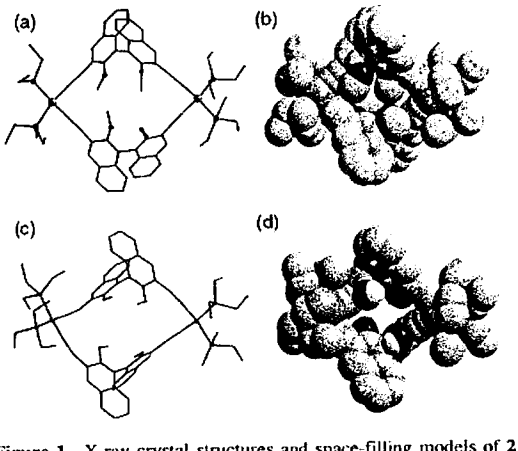

Figure 1. X-ray crystal structures and space-filling models of 2 (a and b) and 4 (c and d). In 2, average Pt–C distance is 1.99 Å, average Pt–P distance is 2.30 Å, average C–Pt–C angle is 86.0°, and average P–Pt–P angle is 100.9°. In 4, average Pt–C distance is 1.988 Å, average Pt–P distance is 2.309 Å, average C–Pt–C angle is 86.0°, and average P–Pt–P angle is 101.6°.

Table 1. Asymmetric Diethylzinc Additions to Aromatic Aldehydes Catalyzed by a Combination of 5 or L_6 and $Ti(O^iPr)_4$[a]

aldehyde	conversion	e.e. (%) for 5	e.e. (%) for L_6
	>95%	80.5	59.9
	>95%	87.1	61.1
	>95%	81.2	56.6
	>95%	91.4	59.6
	>95%	78.9	59.3

[a] All reactions were carried out with 10% 5 and 20 equiv of $Ti(O^iPr)_4$ relative to the chiral dihydroxy groups for 16 h. Conversions and ee values were determined by integrations of the GC peaks with a Supelco β-Dex chiral GC column.

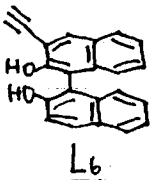

L_6

Chem. Commun. 2002, 96.
6,6'-derivatives

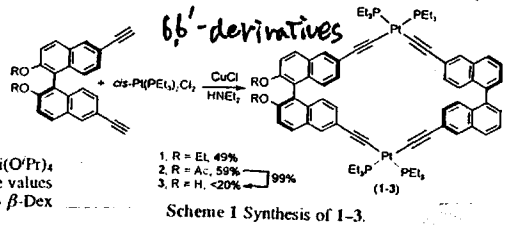

Scheme 1 Synthesis of 1–3.

A Homochiral Porous Metal–Organic Framework for Highly Enantioselective Heterogeneous Asymmetric Catalysis

Chuan-De Wu, Aiguo Hu, Lin Zhang, and Wenbin Lin*

JACS. ASAP
(web release, June 4, 2005)

Chart 1

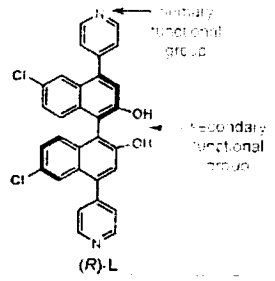

(*R*)-L

$+ 2CdCl_2 \xrightarrow[Et_2O,\ 3days]{DMF/MeOH}$ Colorless crystals → $[Cd_3Cl_6L_3]\cdot 4DMF\cdot 6MeOH\cdot 3H_2O$

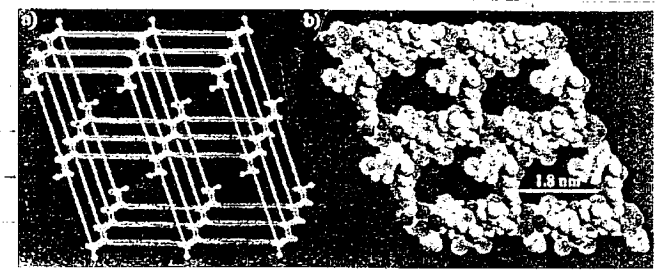

Figure 1. Crystal structure of **1**. Cyan, green, red, blue, gray, and white represent Cd, Cl, O, N, C, and H atoms, respectively. (a) Schematic representation of the 3D framework of **1** as viewed slightly off the *a*-axis. The 3D network is formed by linking the $[Cd(\mu\text{-}Cl)_2]_n$ SBUs (zigzag chains shown in purple) with the **L** ligands shown in yellow sticks and pairs of blue sticks. (b) Space-filling model of **1** as viewed down the *a*-axis showing the large chiral 1D channels (~1.6 × 1.8 nm).

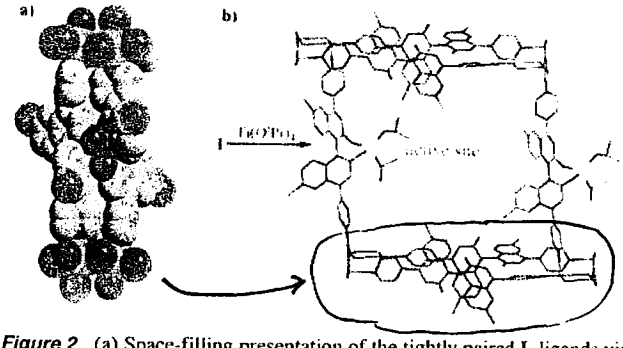

Figure 2. (a) Space-filling presentation of the tightly paired **L** ligands via strong hydrogen bonding and $\pi\cdots\pi$ interactions. (b) Schematic representation of the active (BINOLate)$Ti(O^iPr)_2$ catalytic sites in the open channels of **1**. Cyan, green, red, blue, gray, and yellow represent Cd, Cl, O, N, C, and Ti atoms, respectively.

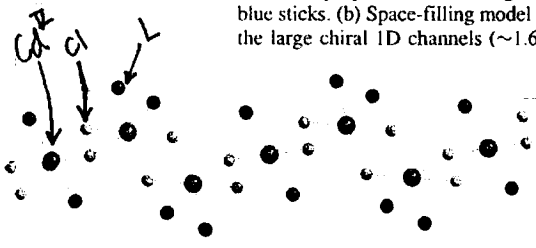

Figure S1 A view of the $[Cd(\mu\text{-}Cl)_2]_n$ zigzag chain secondary building unit in 1

- OH groups for these two L ligands are shielded from the open channels by the naphtyl rings.

- Chiral porous Metal-Organic Framework (MOF)

for the first example of application for asymmetric catalysis, see: Nature, 2000, 404, 982.
(for transesterification, ~8% ee was obtained.)

- $Ti(O\text{-}iPr)_4$ + 1 → heterogeneous catalyst.

(The supernatant from a mixture of 1 and $Ti(O\text{-}i\text{-}Pr)_4$ did not promote the reaction.)

- No $ZnEt_2$ addition product was observed for the largest aldehyde 4′-G_2′-PhCHO.

⇓

The reaction should occur in the open channel of the heterogeneous catalyst.

- Selectivity by the size of substrates.

Table 1. Ti(IV)-Catalyzed $ZnEt_2$ Additions to Aromatic Aldehydes[a]

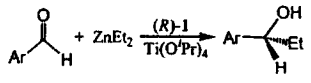

	BINOL/$Ti(O^iPr)_4$		1·Ti	
Ar	conv %	ee %	conv %	ee %
1-Naph	>99	94	>99	93
Ph	>99	88	>99	83
4-Cl–Ph	>99	86	>99	80
3-Br–Ph	>99	84	>99	80
4′-G_0OPh	>99	80	>99	88
4′-G_1′OPh	>99	75	73	77
4′-G_1OPh	>99	78	63	81
4′-G_2′OPh	95[b]	67[b]	0	–

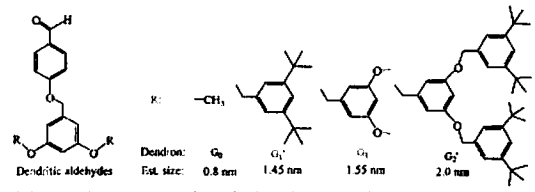

[a] All the reactions were conducted with 13 mol % of **1** or 20 mol % BINOL and excess amounts of $Ti(O^iPr)_4$ at room temperature for 12 h. Conv % were determined by GC or NMR, while ee % values were determined on chiral GC or HPLC for all the secondary alcohols except for 4′-G_2′OPh whose ee % was determined by NMR spectrum of its Mosher's ester. [b] With 40 mol % BINOL.

(b). Artificial Ion Channel (Rigid-Rod β-Barrels)
Stefan Matile et al. Reviews: Acc. Chem. Res. 2005, 38, 79.
Chem. Commun. 2003, 2514.

ORGANIC LETTERS
2001
Vol. 3, No. 26
4229–4232

p-Octiphenyl β-Barrels with Ion Channel and Esterase Activity

Bodo Baumeister, Naomi Sakai, and Stefan Matile*

" Synthetic Multifunctional Pores "

Self-assembly of p-octylphenyls in water or in lipid bilayer membrane.

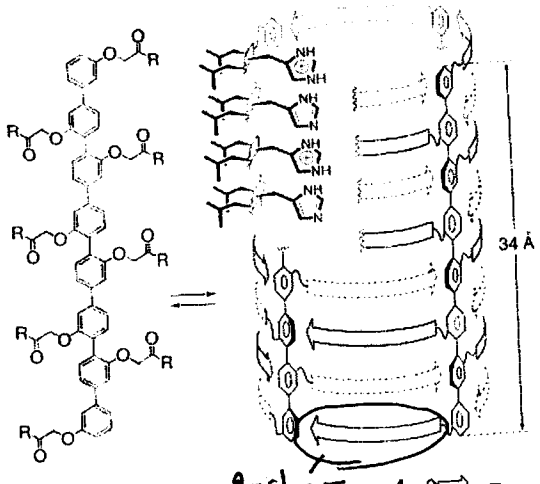

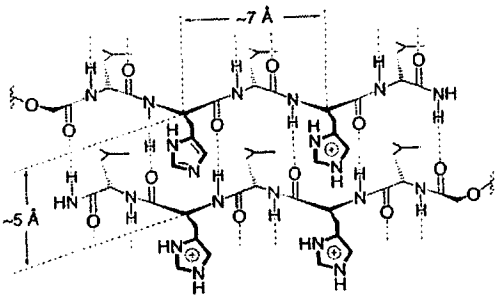

Figure 1. Structure of *p*-octiphenyl **1** and designed cutaway suprastructure of rigid-rod β-barrel 1^4 with pertinent distances estimated from molecular models. The extent of protonation of internal histidines depends on pH and is indicated arbitrarily. Four histidine residues from two β-strands forming a rectangle of ~5 Å × ~7 Å are named "H-quartet" for convenience only (bottom).

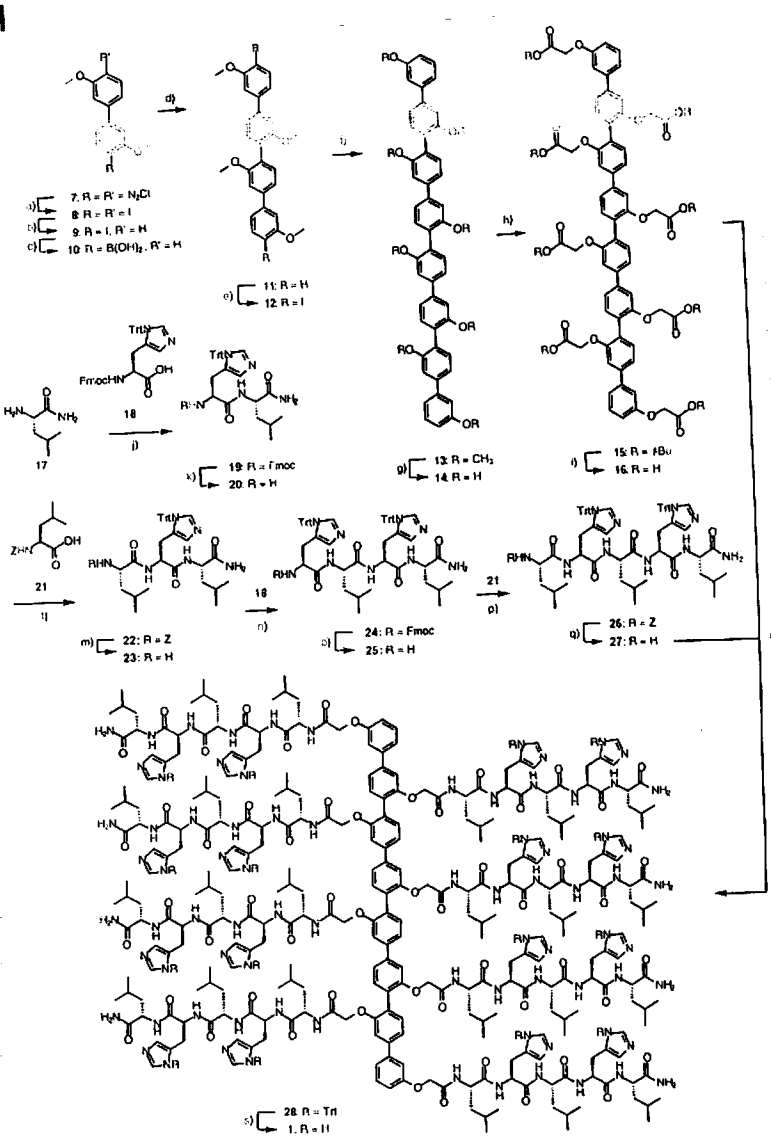

(a) KI, 70%. (b) 1. ^{t}BuLi, 2. H_2O, 67%. (c) 1. ^{t}BuLi, 2. $B(O^iPr)_3$, 3. H_2O, 75%. (d) 1. 9, ^{t}BuLi, $CuCl_2$, 64%. (e) 1. ^{t}BuLi, 2. I_2, 46%. (f) 10, $Pd(PPh_3)_4$, Na_2CO_3, 66%. (g) BBr_3. $BrCH_2COO^tBu$, Cs_2CO_3, 69% from 13. (i) TFA. (j) EDC, HOBt, TEA, 94%. (k) piperidine, 91 (l) EDC, HOBt, TEA, 80%. (m) H_2, Pd/C, 90%. (n) EDC, HOBt, TEA, 89%. (o) piperidi quant. (p) EDC, HOBt, TEA, 89%. (q) H_2, Pd/C, 80%. (r) HBTU, TEA, 58% from 15. (s) T quant.

- all hydrophobic leucine side chains place at the outer barrel surface to intact with lipid bilayer
- the hydrophilic histidine residues point inward to form a transmembrane channel.
- 1^n self-assembles spontaneously in aqueous media at concentrations below 3 μM.

Scheme 1

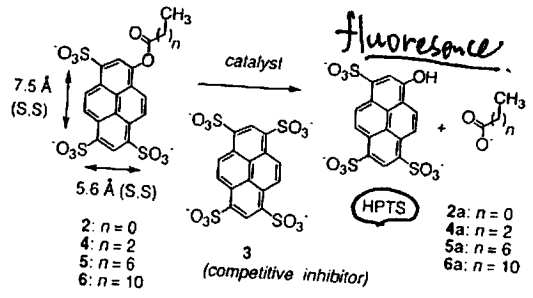

a) 1^4: ToN > 120

b) highest catalyst activity at pH 5.5.

) The esterolytic activity of rigid-rod β-barrel 1^4 was independent of presence or absence of spherical bilayer membranes composed of egg yolk phosphatidylcholine.

d) This indicated that anion 3 acts as a competitive inhibitor

e) Increased of the substrate hydrophobicity caused higher Michaelis constant (i.e., lower binding affinity)

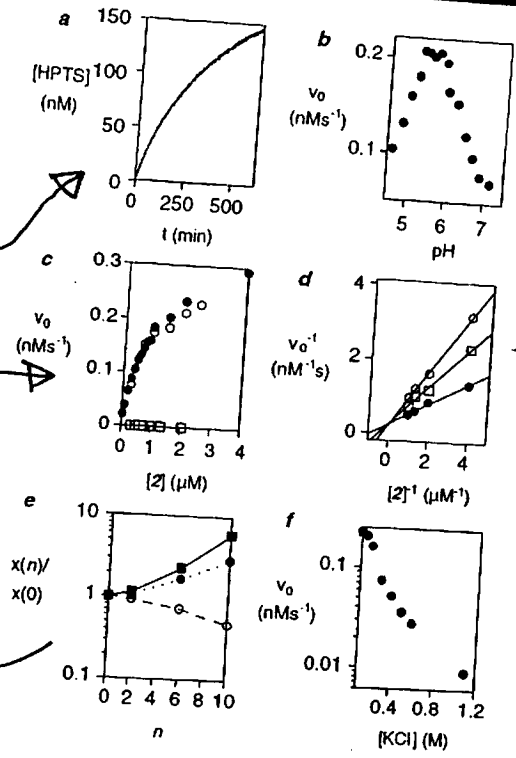

Figure 2. Esterolytic activity of β-barrels 1^4. (*a*) Increase in product concentration (HPTS, λ_{em} = 510 nm, λ_{ex} = 415.5 nm; controls, 404 nm, 455 nm) as a function of time (1 μM **2**, 1.35 nM 1^4, pH 5.5). (*b*) Initial velocities of product formation as a function of pH. (*c*) Substrate concentration in the presence (●) and absence (○) of EYPC bilayer membranes (10 mM EYPC) compared to 540 nM MeIm (□). (*d*) Lineweaver–Burk plots in the presence of 0 μM (●), 0.5 μM (□), and 1.0 μM (○) inhibitor **3**. (*e*) hydrophobicity – plot of kinetic constants x (n) = K_M (■), k_{cat} (●), and k_{cat}/K_M (○) for substrates **2** (n = 0, x (0)), **4** (n = 2), **5** (n = 6), and **6** (n = 10). (*f*) Initial velocities of product formation as a function of KCl concentration. Conditions, if not varied as indicated: 135 nM β-barrel 1^4, 2 μM **2**, 10 mM MES, 100 mM KCl, pH 5.5, rt, dark.

c) JACS, 2004, 126, 10067.

JACS. ASAP
(web release June 10, 2005)

Sugar Sensing with Synthetic Multifunctional Pores

Svetlana Litvinchuk, Nathalie Sordé, and Stefan Matile*

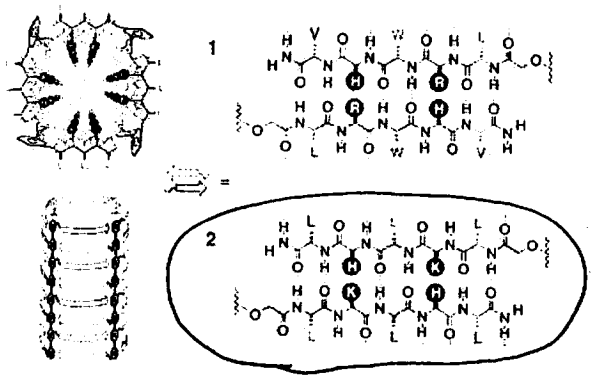

Figure 1. Notional rigid-rod β-barrel pores **1** and **2** with β-sheets as solid (backbone) and dotted lines (hydrogen bonds, top) or as arrows (N → C, bottom). External amino acid residues are dark on white, and internal ones are white on dark (single-letter abbreviations).

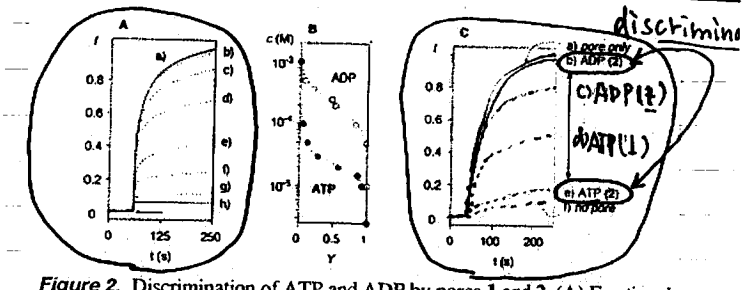

Figure 2. Discrimination of ATP and ADP by pores **1** and **2**. (A) Fractional change in CF emission I (λ_{ex} 492 nm, λ_{em} 517 nm) as a function of time after addition of ATP (0 (a), 1 (b), 10 (c), 20 (d), 30 (e), 50 (f), 100 (g), and 1000 μM (h) and barrel **2** (94 nM tetramer; arrow) to EYPC-LUVs⊃CF (65 μM EYPC, 10 mM HEPES, 107 mM NaCl, pH 6.5). (B) Dose-response curves for blockage of pore **2** by ATP (●) and ADP (○) with fit to the Hill equation. (C) As in A with 10 μM $MgCl_2$,[10] without (a) or with 100 μM ADP (b) and 100 μM ATP (e) for pore **2** compared to previous data[2] for blockage of pore **1** with equimolar amounts of ADP (c) and ATP (d).

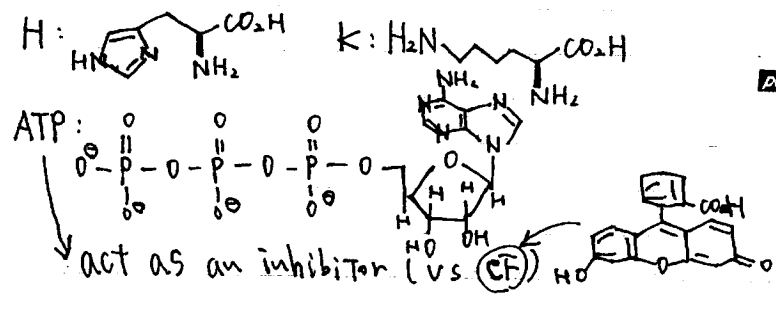

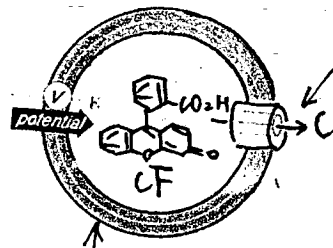

ATP·ADP-blockage

ex.) Fig 2A

ATP ↑ → fluoresence ↓

large unilamellar vesicles composed of egg yolk phosphatidylcholine

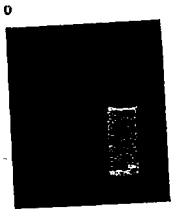

(D) Emission after addition of pore **2** (94 nM) to 1 mL of Coca-Cola Light (left) and Coca-Cola (right) diluted with (a) invertase (3×; 16 units/mL; 50 mM NaOAc/AcOH, pH 4.5, 55 °C, 10 min), (b) ATP (20×; 10 mM; 0.7 units/mL hexokinase, 10 mM $MgCl_2$, 100 mM Tris, pH 8, 30 °C, 40 min), and (c) EYPC-LUVs⊃CF (100×), excitation with UV lamp at 366 nm, detected ≤30 min after pore addition.

· Sugar Sensor

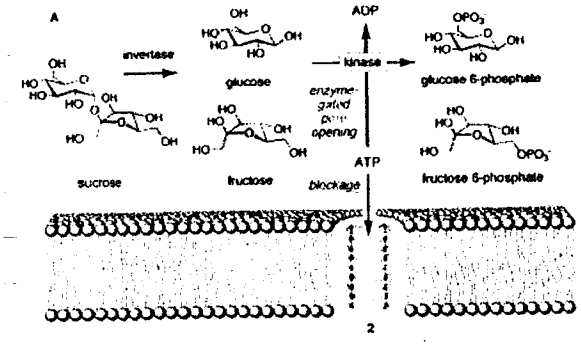

Table 1. Sucrose Content of Soft Drinks Determined with Pore **2**[a]

	beverage	expected (gL^{-1})	found (gL^{-1})
1	Coca-Cola	106	111 ± 7
2	Coca-Cola Light	0	0
3	Red Bull	113	118 ± 13
4	Fanta Orange	101	98 ± 9
5	Nestea Lemon	76	78 ± 7

[a] See Figure 1 for structures and Figure 3 for method.

Soft drinks (diluted) + invertase
↓
ATP + hexokinase
↓
EYPC-LUVs⊃CF
↓
2 → fluorescence

Previous report.
Cf. Science, 2002, 298, 1600.

i.e., ATP

B

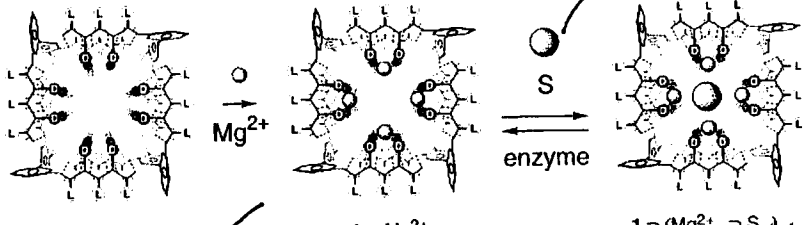

1 — **1** ⊃ $Mg^{2+}{}_n$ (active pore) — **1** ⊃ $(Mg^{2+}{}_n \supset S_n)_n$ (inactive pore)

D: HO_2C (CH) CO_2H, NH_2

· chiral metal complex with β-barrel structure.

·

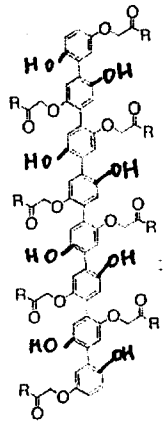

1: R = -LHLHL-NH_2

p-octiphenyls — non planar structure.
↓
… biphenyldiol-type ligand ??

Chiral catalytic pore ?